

# dynActivation: A Trainable Activation Family for Adaptive Nonlinearity

Alois Bachmann  
Ruprecht-Karls-Universität Heidelberg  
alois.bachmann@stud.uni-heidelberg.de

21st of March 2026

## Abstract

Standard activation functions impose a fixed nonlinearity on every layer of a neural network. This paper proposes *dynActivation*, a per-layer trainable activation defined as  $f_i(x) = \text{BaseAct}(x)(\alpha_i - \beta_i) + \beta_i x$ , where  $\alpha_i$  and  $\beta_i$  are lightweight learned scalars that interpolate between the base nonlinearity and a linear path and  $\text{BaseAct}(x)$  resembles any ReLU-like function. The static and dynamic ReLU-like variants are then compared across multiple vision tasks, language modeling tasks, and ablation studies. The results suggest that dynActivation variants tend to linearize deep layers while maintaining high performance, which can improve training efficiency by up to +54% over ReLU.

On CIFAR-10 [14], dynActivation(Mish) improves over static Mish [1] by up to +14.02% on AttentionCNN [23] with an average improvement by +6.00%, with a 24% convergence-AUC reduction relative to Mish (2120 vs. 2785). In a 1-to-75-layer MNIST [15] depth-scaling study, dynAct never drops below 95% test accuracy (95.3–99.3%), while ReLU collapses below 80% at 25 layers. Under FGSM [9] at  $\varepsilon=0.08$ , dynActivation(Mish) incurs a 55.39% accuracy drop versus 62.79% for ReLU (7.40% advantage). Transferred to language modeling, a new proposed dynActGLU(Swish)-variant achieves a 10.3% relative perplexity reduction over SwiGLU [13] at 5,620 steps (4.047 vs. 4.514), though the gap vanishes at 34,300 steps.

## Contents

<b>1</b>	<b>Introduction</b>	<b>3</b>
<b>2</b>	<b>Motivation</b>	<b>3</b>
2.1	Why trainable activations . . . . .	3
2.2	Local intuition figure pair . . . . .	4
<b>3</b>	<b>dynActivation</b>	<b>4</b>
3.1	Derivation . . . . .	4
3.2	Parameter interpretation . . . . .	5
3.3	Gradient and parameter analysis . . . . .	5
3.4	Gradient-flow / Lipschitz figure pair . . . . .	6
<b>4</b>	<b>Experimental Setup</b>	<b>6</b>
4.1	Protocol . . . . .	6
4.2	Architectures and datasets . . . . .	6
<b>5</b>	<b>CIFAR Validation</b>	<b>7</b>
5.1	Environment Setup . . . . .	7
5.2	dynActivation variants comparison . . . . .	7
5.3	Best-per-combination test . . . . .	7
5.4	Full comparison . . . . .	8

5.5	Extended activation comparison . . . . .	9
5.6	Statistical significance tests . . . . .	10
5.7	Local figure + local interpretation . . . . .	11
<b>6</b>	<b>Overfitting Analysis on MNIST</b>	<b>12</b>
6.1	Experimental setup for MNIST depth scaling . . . . .	12
6.2	Depth scaling figure pair . . . . .	12
6.3	Learned activation visualization . . . . .	13
6.4	Interpretation . . . . .	13
<b>7</b>	<b>LLM Transfer Experiments</b>	<b>13</b>
7.1	dynActGLU formulation . . . . .	13
7.2	Short-run table . . . . .	14
7.3	Long-run table . . . . .	14
<b>8</b>	<b>Unified Evaluation</b>	<b>14</b>
8.1	Stability tests . . . . .	14
8.1.1	Initialization stability . . . . .	14
8.1.2	Optimizer-/init-stability test . . . . .	15
8.1.3	Hyperparameter-stability test . . . . .	15
8.1.4	Monotonicity / curvature test . . . . .	15
8.2	Robustness tests . . . . .	16
8.2.1	Distribution-shift test . . . . .	16
8.2.2	Adversarial-robustness test . . . . .	16
8.2.3	Regularization ablation . . . . .	17
8.3	Efficiency tests . . . . .	18
8.3.1	Convergence test . . . . .	18
8.3.2	Runtime benchmark . . . . .	18
8.3.3	Training-efficiency test . . . . .	19
<b>9</b>	<b>Discussion</b>	<b>20</b>
<b>10</b>	<b>Limitations</b>	<b>20</b>

# 1 Introduction

Activation functions are a small but influential component of modern neural networks. Although they contribute few or no trainable parameters relative to the full model, they strongly affect gradient propagation, optimization stability, and final performance. In practice, however, activation functions are still chosen as fixed design decisions rather than learned components.

This paper proposes *dynActivation*, a trainable activation family defined as  $f_i(x) = \text{BaseAct}(x)(\alpha_i - \beta_i) + \beta_i x$ , where  $\alpha_i$  and  $\beta_i$  are per-layer scalars learned alongside the standard model weights. This preserves the inductive bias of established base activations such as Mish, GELU, Swish, or ReLU while allowing each layer to adapt its effective nonlinearity.

One possible explanation for the improvements is that the additional linear path  $\beta_i x$  appears to provide a gradient highway in layers where strong nonlinearity impedes information transport, while layers that benefit from high curvature retain it.

The experiments validate *dynActivation* through CIFAR [14] image classification benchmarks, a 1-to-75-layer MNIST depth-scaling study, LLM transfer experiments, and a unified evaluation spanning adversarial robustness, optimizer stability, distribution-shift resilience, convergence, and ablations.

The main contributions are:

- **Formulation and interpretation.** This work derives *dynActivation* and provides a gradient-based interpretation showing how the linear path controlled by  $\beta_i$  acts as a gradient highway.
- **CIFAR validation.** In a broad comparison *dynActivation*(Mish) achieves the highest mean accuracy on CIFAR-10 with statistical significant improvements over its static counterpart and up to improvements of +14.02 pp over static Mish [1] on CIFAR-10/AttentionCNN and +12.39 pp over ReLU [2] on CIFAR-100/AttentionCNN.
- **Depth scaling.** On MNIST, *dynAct* maintains  $> 95\%$  test accuracy from 1 to 75 layers, while ReLU collapses below 80% at 25 layers.
- **Convergence.** *dynActivation*(Mish) reduces training-loss AUC by 24% relative to static Mish (2120 vs. 2785).
- **Adversarial robustness.** Under FGSM [9] at  $\varepsilon=0.08$ , *dynActivation*(Mish) reduces accuracy drop by 7.40 pp versus ReLU, 8.28 pp versus Mish, and 8.56 pp versus Swish.
- **Optimizer-initialization stability.** Across 27 optimizer-init-learning-rate configurations on CIFAR-10/ResNet18 [5], *dynActivation*(Mish) achieves mean accuracy 52.81%, outperforming Mish by +3.34 pp and ReLU by +10.56 pp.
- **LLM transfer.** *dynActGLU*(Swish) reduces perplexity by 10.3% relative to SwiGLU [13] after 5,620 training steps, with no meaningful regression at 34,300 steps.

## 2 Motivation

### 2.1 Why trainable activations

A fixed activation imposes one global functional shape on all layers, regardless of their depth or role. Early, middle, and late layers may require different levels of nonlinearity, yet standard activations such as ReLU [2], GELU [3], Swish [4], and Mish [1] remain fixed once selected. Recent work has further explored non-monotonic and smooth activation designs [21, 22]. *dynActivation* lets the network adapt the effective shape of a chosen base activation during training while keeping the additional parameter count to two scalars per layer.

## 2.2 Local intuition figure pair

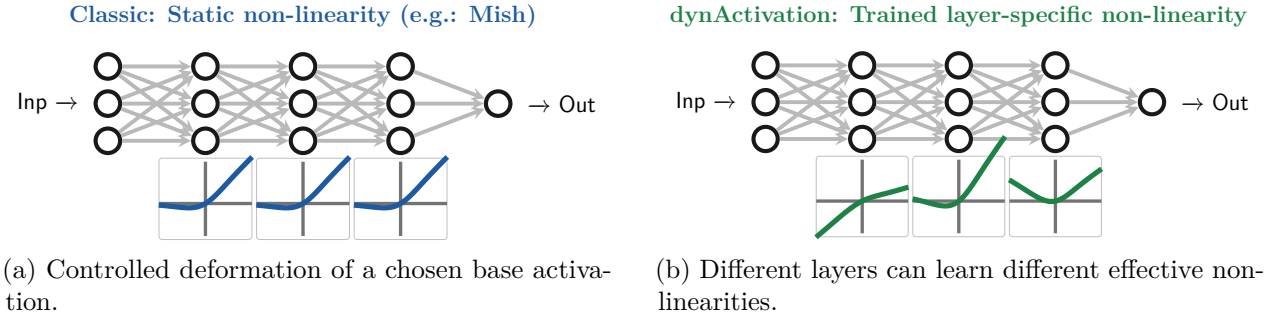


Figure 1: Motivational view of trainable activations.

## 3 dynActivation

### 3.1 Derivation

A piecewise-linear activation can be interpreted as having two arms, one for negative and one for positive inputs. Allowing these arms to move independently would let the activation adapt its effective slope, but a hard piecewise construction would be non-smooth and less suitable for gradient-based optimization.

To avoid this, the construction begins with a smooth sigmoid-based gating mechanism. After combining both branches and simplifying, the result takes the form of a Swish-like term plus an explicitly linear term. Replacing the sigmoid-based base term by a general  $\text{BaseAct}(x)$  turns the construction into a family of trainable activations.

The resulting activation for layer  $i$  is

$$f_i(x) := \text{BaseAct}(x) \cdot (\alpha_i - \beta_i) + \beta_i x. \quad (1)$$

This formulation keeps the base activation as the main nonlinear component while allowing two trainable parameters to adapt its effective contribution and its linear correction.

**Derivation:**

$$\sigma(x) = \frac{1}{1 + e^{-x}} \quad (2)$$

$$\text{dynSigmoid}_{\text{right}}(x) = \sigma(x)\alpha \quad (3)$$

$$\text{dynSigmoid}_{\text{left}}(x) = (\sigma(x) - 1)\beta \quad (4)$$

$$\text{dynActivation}(x) = \sigma(x)x(\alpha - \beta) + \beta x \quad (5)$$

$$\Rightarrow \text{BaseAct}(x)(\alpha - \beta) + \beta x \quad (6)$$

The special case  $\text{dynAct}(x) := \text{dynActivation}(x; \text{BaseAct} = \text{Mish})$  serves as the default variant in several experiments, motivated by its strong average performance and stability in the comparative benchmarks.

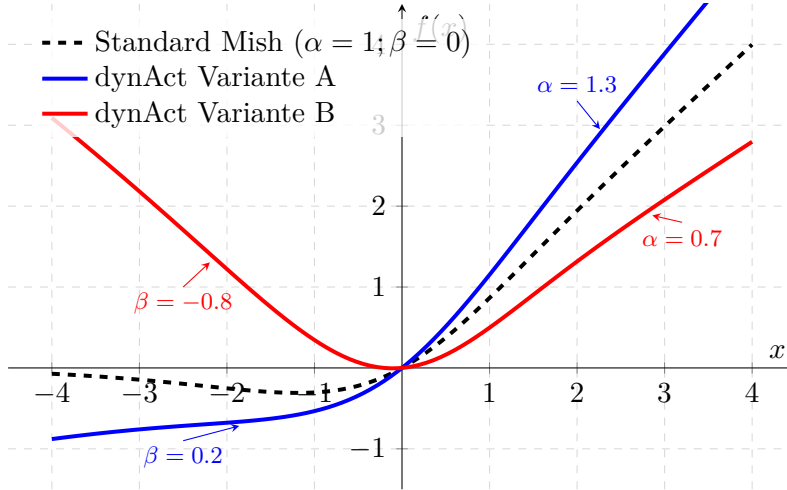


Figure 2: Schematic view of the dynActivation family and its shape deformation relative to the base activation.

Table 1: Core definitions of the dynActivation family.

Object	Definition / interpretation
BaseAct( $x$ )	Chosen base activation, e.g. Mish, GELU, Swish, or ReLU.
$\alpha_i$	Trainable per-layer coefficient scaling the base activation contribution.
$\beta_i$	Trainable per-layer coefficient defining the explicit linear path.
$f_i(x)$	$\text{BaseAct}(x) \cdot (\alpha_i - \beta_i) + \beta_i x$ .
dynAct( $x$ )	Special case using Mish as base activation.

### 3.2 Parameter interpretation

The parameter  $\alpha_i$  controls how strongly the base activation contributes to the resulting function, whereas  $\beta_i$  introduces an explicit linear component. When  $\alpha_i \approx 1$  and  $\beta_i \approx 0$ , dynActivation stays close to the original base activation. When  $\alpha_i \approx \beta_i$ , the nonlinear contribution is reduced and the function becomes approximately linear.

### 3.3 Gradient and parameter analysis

The gradient structure of dynActivation provides the key intuition for why the activation may improve training behavior. From the definition, the derivative yields

$$\frac{\partial f_i}{\partial x} = \text{BaseAct}'(x) \cdot (\alpha_i - \beta_i) + \beta_i, \quad (7)$$

$$\frac{\partial f_i}{\partial \alpha_i} = \text{BaseAct}(x), \quad (8)$$

$$\frac{\partial f_i}{\partial \beta_i} = x - \text{BaseAct}(x). \quad (9)$$

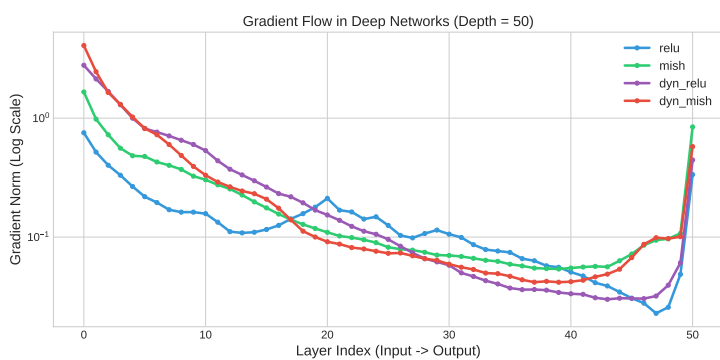
The additive  $\beta_i$  term in  $\partial f_i / \partial x$  creates a linear gradient path independent of the base activation’s derivative. The model can therefore learn a more direct transport path whenever the optimization problem benefits from it, offering a plausible explanation for improved convergence or greater stability in deeper networks.

The update for  $\alpha_i$  is driven directly by the base activation output, while the update for  $\beta_i$  depends on the difference between the identity path and the base activation. Initializing  $\beta_i = 0$  does not freeze the parameter, because its gradient does not vanish at that initialization.

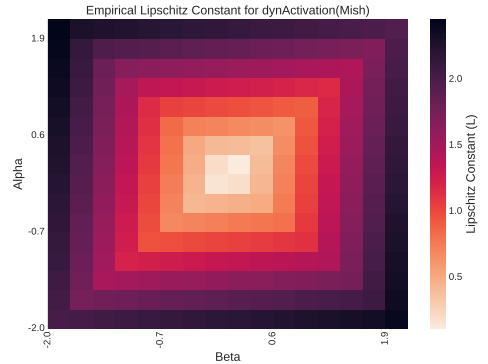
### 3.4 Gradient-flow / Lipschitz figure pair

Figure 3 (left) provides a qualitative comparison of gradient-flow behavior across depth in a 50-layer network. Compared with the static activations, the dynamic variants show less severe gradient decay through much of the network, especially beyond the early layers. This suggests that the learned linear component can help preserve gradient propagation, although the effect is best interpreted qualitatively rather than through exact ratios read from the plot.

Figure 3 (right) shows the empirical Lipschitz landscape of dynActivation as a function of  $(\alpha, \beta)$ . The plot indicates a broad region of moderate Lipschitz values surrounded by larger values toward the edges of the parameter space. The parameters reached during training fall within this moderate region, supporting the claim that the learned activation typically operates away from obviously unstable settings.



(a) Gradient flow over normalized depth.



(b) Lipschitz behavior over parameter settings.

Figure 3: Gradient flow and Lipschitz behavior of dynActivation.

## 4 Experimental Setup

### 4.1 Protocol

All experiments follow a reproducible protocol with fixed seeds, explicitly reported training settings, and architecture-specific benchmark configurations. Classification results are reported using test accuracy and test loss, while additional modules report metrics such as corruption robustness, adversarial robustness, convergence AUC, and efficiency measurements.

System	GPU (VRAM)	CPU	RAM	SSD
System 1	RTX 2080 Ti (11 GB)	Ryzen 7 5700X CPU	32 GB DDR4	1 TB
System 2 (Cloud)	RTX 5090 (32 GB)	AMD EPYC 7763	112.8 GB DDR4	16 GB

Table 2: Hardware specification of Training Systems.

### 4.2 Architectures and datasets

The evaluation uses CIFAR-10 and CIFAR-100 [14] as the main image-classification benchmarks. MNIST [15] serves for the depth-scaling and overfitting analysis because its relative simplicity makes depth-dependent degradation easier to observe. Language-model transfer is tested in a Monad-70M [20] setting on the SYNTH dataset through a dynActGLU formulation. The unified suite combines results from robustness, calibration, efficiency, and ablation modules across multiple architectures.

The compared activations include both standard and dynamic variants. In the main CIFAR comparisons, the paper considers ReLU, GELU, SiLU, Mish [1], and their dynamic counterparts. The extended comparison broadens this set to include ELU [39], PReLU [6], SELU [8], and others.

## 5 CIFAR Validation

### 5.1 Environment Setup

Setting	Value
Framework	PyTorch
Optimizer	Adam [12]
Learning rate	0.001
Weight decay	5e-9
Scheduler	StepLR(step_size=10, gamma=0.1)
Gradient clipping	clip_grad_norm(..., max_norm=1.0)
CIFAR batch size	128
MNIST batch size	256
CIFAR epochs	30
Statistical runs	5 seeds per architecture-dataset-activation combination
Augmentation	RandomCrop(32, padding=4), RandomHorizontalFlip, dataset-specific normalization

Table 3: Experimental protocol and reproducibility settings.

### 5.2 dynActivation variants comparison

Table 4 reports the average performance across all seven dataset–architecture combinations. `dynActivation(Mish)` leads with a mean accuracy of 66.86% ( $\sigma = 0.58$ ), followed by `dynActivation(GELU)` at 66.69% (−0.17 pp deficit), `dynActivation(SiLU)` at 65.65%, and `dynActivation(ReLU)` at 60.91% (−5.95 pp). The lowest standard deviation for `dynActivation(Mish)` ( $\sigma = 0.58$  vs. 1.99 for `dynActivation(ReLU)`) indicates that the Mish base not only achieves the highest mean but is also the most consistent across configurations. These results identify `dynActivation(Mish)` as the recommended default within the `dynActivation` family, while leaving open the possibility of local improvements from other base activations on specific architectures.

Activation	Mean Acc	Std Acc	Mean Loss	Std Loss
<code>dynActivation(Mish)</code>	66.8571	0.5845	1.1781	0.0235
<code>dynActivation(GELU)</code>	66.6886	0.7935	1.1810	0.0312
<code>dynActivation(SiLU)</code>	65.6500	1.1292	1.2304	0.0365
<code>dynActivation(ReLU)</code>	60.9117	1.9969	1.4215	0.0998

Table 4: Average performance over all dataset–architecture combinations for the dynamic variants.

### 5.3 Best-per-combination test

Table 5 reports the best dynamic activation separately for each dataset–architecture combination.

`dynActivation(Mish)` wins 5 out of 7 dataset–architecture combinations. The performance gains range from +0.79 pp on CIFAR-10/MobileNet [16] (over GELU) to +14.02 pp on CIFAR-10/AttentionCNN over static Mish and +4.63 pp over ReLU on the same combination. On CIFAR-10/DenseNet [17], `dynActivation(Mish)` improves ReLU by +1.76 pp. `dynActivation(GELU)` is locally superior on CIFAR-10/ResNet18 and CIFAR-100/AttentionCNN, the latter achieving 45.70% vs. 33.31% for ReLU (+12.39 pp), the single largest margin in the study.

Dataset	Architecture	Best dynActivation	Mean Acc	Mean Loss
CIFAR10	AttentionCNN	dynActivation(Mish)	78.27	0.6390
CIFAR10	DenseNet	dynActivation(Mish)	81.92	0.5466
CIFAR10	MobileNet	dynActivation(Mish)	80.87	0.5743
CIFAR10	ResNet18	dynActivation(GELU)	84.11	0.5196
CIFAR100	AttentionCNN	dynActivation(GELU)	45.70	2.0433
CIFAR100	DenseNet	dynActivation(Mish)	52.42	1.7713
CIFAR100	MobileNet	dynActivation(Mish)	45.39	2.1282

Table 5: Best dynamic variant per dataset-architecture combination.

## 5.4 Full comparison

The comparison emphasizes both mean accuracy and seed-to-seed dispersion. The single largest gain appears on CIFAR-100/AttentionCNN, where dynActivation(GELU) reaches 45.70% versus 33.31% for ReLU, a margin of +12.39 pp. On CIFAR-10/AttentionCNN, dynActivation(Mish) at 78.27% exceeds static Mish (64.25%, -14.02 pp) and ReLU (73.64%, -4.63 pp) while also reducing standard deviation from 1.43 to 0.85. Across the full table, every dynamic variant improves upon at least one static baseline in its winning combination, and none exhibits the variance inflation seen in dynActivation(ReLU) at the variant level.

Table 6: CIFAR-Statistics: Comparisons of the activations per combination.  $\Delta\text{Acc}/\Delta\text{Loss}$  are relative to the best dynActivation-variant for the specific combination.

Aktivierung	Mean Acc (%)	$\sigma(\text{Acc})$	Mean Loss	$\sigma(\text{Loss})$	$\Delta\text{Acc}$	$\Delta\text{Loss}$
<b>CIFAR10 – AttentionCNN</b>						
ReLU	73.64	1.4321	0.7605	0.0497	-4.63	+0.1215
GELU	69.83	1.7864	0.8624	0.0542	-8.44	+0.2234
Mish	64.25	1.6702	1.0001	0.0508	-14.02	+0.3611
SiLU	63.95	1.2492	1.0086	0.0323	-14.32	+0.3696
<b>dynActivation(Mish)</b>	<b>78.27</b>	<b>0.8523</b>	<b>0.6390</b>	<b>0.0259</b>	+0.00	+0.0000
<b>CIFAR10 – DenseNet</b>						
ReLU	80.16	0.6478	0.5868	0.0212	-1.76	+0.0402
GELU	80.83	0.9647	0.5637	0.0330	-1.09	+0.0171
Mish	80.20	0.7894	0.5888	0.0258	-1.72	+0.0422
SiLU	80.45	<b>0.4493</b>	0.5835	0.0205	-1.47	+0.0369
<b>dynActivation(Mish)</b>	<b>81.92</b>	<b>0.4494</b>	<b>0.5466</b>	<b>0.0151</b>	+0.00	+0.0000
<b>CIFAR10 – MobileNet</b>						
ReLU	77.93	1.4169	0.6719	0.0582	-2.94	+0.0976
GELU	80.08	0.5638	0.5886	<b>0.0134</b>	-0.79	+0.0143
Mish	79.16	0.6710	0.6209	0.0246	-1.71	+0.0466
SiLU	79.05	<b>0.3782</b>	0.6212	0.0138	-1.82	+0.0469
<b>dynActivation(Mish)</b>	<b>80.87</b>	0.4648	<b>0.5743</b>	0.0178	+0.00	+0.0000
<b>CIFAR10 – ResNet18</b>						
ReLU	83.54	0.2272	0.4991	<b>0.0059</b>	-0.57	-0.0205
GELU	84.07	<b>0.1581</b>	0.4988	0.0093	-0.04	-0.0208

Continuation on the next page.

Aktivierung	Mean Acc (%)	$\sigma(\text{Acc})$	Mean Loss	$\sigma(\text{Loss})$	$\Delta\text{Acc}$	$\Delta\text{Loss}$
Mish	83.97	0.2868	<b>0.4920</b>	0.0086	-0.14	-0.0276
SiLU	83.95	0.1927	0.4935	0.0063	-0.16	-0.0261
dynActivation(Mish)	84.02	0.3222	0.5276	0.0106	-0.09	+0.0080
<b>dynActivation(GELU)</b>	<b>84.11</b>	0.3765	0.5196	0.0111	+0.00	+0.0000
<b>CIFAR100 – AttentionCNN</b>						
ReLU	33.31	2.5522	2.5215	0.1082	-12.39	+0.4782
GELU	30.69	1.3821	2.6836	0.0852	-15.01	+0.6403
Mish	27.55	1.0424	2.8212	0.0649	-18.15	+0.7779
SiLU	24.65	<b>0.7931</b>	2.9693	0.0345	-21.05	+0.9260
dynActivation(Mish)	45.55	0.9498	2.0463	<b>0.0472</b>	-0.15	+0.0030
<b>dynActivation(GELU)</b>	<b>45.70</b>	1.0976	<b>2.0433</b>	0.0552	+0.00	+0.0000
<b>CIFAR100 – DenseNet</b>						
ReLU	51.18	1.0539	1.8240	0.0399	-1.24	+0.0527
GELU	51.16	0.9901	1.8170	0.0341	-1.26	+0.0457
Mish	48.06	1.9885	1.9529	0.1048	-4.36	+0.1816
SiLU	48.61	0.8971	1.9248	0.0426	-3.81	+0.1535
dynActivation(Mish)	51.98	<b>0.4402</b>	1.7846	<b>0.0124</b>	-0.44	+0.0133
<b>dynActivation(GELU)</b>	<b>52.42</b>	0.7582	<b>1.7713</b>	0.0319	+0.00	+0.0000
<b>CIFAR100 – MobileNet</b>						
ReLU	40.99	1.6794	2.2493	0.0794	-4.40	+0.1211
GELU	44.07	0.9372	<b>2.1049</b>	0.0451	-1.32	-0.0233
Mish	42.82	0.7421	2.1509	0.0316	-2.57	+0.0227
SiLU	42.24	<b>0.2910</b>	2.1806	<b>0.0134</b>	-3.15	+0.0524
<b>dynActivation(Mish)</b>	<b>45.39</b>	0.6126	2.1282	0.0353	+0.00	+0.0000

## 5.5 Extended activation comparison

To avoid drawing conclusions from too narrow a baseline set, the comparison extends to a comprehensive group of 27 standard and recent trainable activations—including variants such as Apa, MELU, PReLU, and TAAF.

As reported in Table 7, dynActivation(Mish) achieves the highest overall accuracy at  $79.72 \pm 0.0073$ , improving on its static base activation Mish ( $78.91 \pm 0.0041$ , a  $+0.81$  pp improvement) and outperforming recent trainable alternatives like Apa (79.26%) and Trainable\_swish (79.11%). The dynActivation family claims the top three ranks overall, with dynActivation(GELU) and dynActivation(SiLU) achieving 79.69 and 79.52 respectively. Notably, the lowest-performing dynamic variant, dynActivation(ReLU) at 78.22, still outperforms static ReLU (77.66).

Activation	Accuracy (Mean $\pm$ Std)	Loss (Mean $\pm$ Std)	Trainable
Apa [24]	0.7926 $\pm$ 0.0055	0.6287 $\pm$ 0.0178	Yes
Trainable_swish [4]	0.7911 $\pm$ 0.0047	0.6318 $\pm$ 0.0112	Yes
Pdelu [25]	0.7909 $\pm$ 0.0054	0.6474 $\pm$ 0.0217	Yes
Melu [26]	0.7904 $\pm$ 0.0075	0.6597 $\pm$ 0.0258	Yes
Mish [1]	0.7891 $\pm$ 0.0041	0.6348 $\pm$ 0.0108	No
Prelu_scalar [6]	0.7874 $\pm$ 0.0057	0.6740 $\pm$ 0.0136	No
Taaf [27]	0.7874 $\pm$ 0.0047	0.6654 $\pm$ 0.0180	Yes
Adaptive_gelu [3]	0.7871 $\pm$ 0.0044	0.6449 $\pm$ 0.0143	Yes
SiLU [35]	0.7869 $\pm$ 0.0037	0.6368 $\pm$ 0.0109	No
Apl [28]	0.7861 $\pm$ 0.0099	0.6774 $\pm$ 0.0274	Yes
GELU [3]	0.7836 $\pm$ 0.0053	0.6545 $\pm$ 0.0169	No
Hardswish [37]	0.7828 $\pm$ 0.0040	0.6460 $\pm$ 0.0101	No
ELU [39]	0.7814 $\pm$ 0.0032	0.6368 $\pm$ 0.0107	No
CELU [33]	0.7814 $\pm$ 0.0032	0.6368 $\pm$ 0.0107	No
Laaf_relu [29]	0.7785 $\pm$ 0.0066	0.6608 $\pm$ 0.0183	Yes
ReLU [2]	0.7766 $\pm$ 0.0033	0.6615 $\pm$ 0.0102	No
LeakyReLU [34]	0.7765 $\pm$ 0.0055	0.6582 $\pm$ 0.0150	No
Srelu [30]	0.7677 $\pm$ 0.0079	0.7042 $\pm$ 0.0244	Yes
SELU [8]	0.7660 $\pm$ 0.0049	0.6776 $\pm$ 0.0146	No
Softplus [36]	0.7630 $\pm$ 0.0074	0.6798 $\pm$ 0.0186	No
Saaf [31]	0.7556 $\pm$ 0.0062	0.7297 $\pm$ 0.0190	Yes
Tanh [38]	0.7330 $\pm$ 0.0031	0.7723 $\pm$ 0.0094	No
Erfrelu [32]	0.7170 $\pm$ 0.0073	0.8428 $\pm$ 0.0203	Yes
<hr/>			
dynActivation(Mish)	0.7972 $\pm$ 0.0073	0.6720 $\pm$ 0.0214	Yes
dynActivation(GELU)	0.7969 $\pm$ 0.0060	0.6709 $\pm$ 0.0189	Yes
dynActivation(SiLU)	0.7952 $\pm$ 0.0040	0.6738 $\pm$ 0.0154	Yes
dynActivation(ReLU)	0.7822 $\pm$ 0.0031	0.6944 $\pm$ 0.0158	Yes

Table 7: Comparison of standard and dynAct variants, sorted descending by mean accuracy.

## 5.6 Statistical significance tests

Table 8 details the statistical significance of the performance differences measured against the leading activation, dynActivation(Mish). Using a paired t-test over the aggregated combination results, dynActivation(Mish) demonstrates a statistically significant advantage ( $p < 0.05$ ) over the vast majority of the 26 competing functions, including static base activations like Mish ( $p = 0.0375$ ), ReLU ( $p = 0.0205$ ), and closely related trainable variants such as MELU ( $p = 0.0017$ ) and TAAF ( $p = 0.0466$ ).

The statistical test fails to reject the null hypothesis only for a small cluster of highly competitive activations. Specifically, dynActivation(GELU) ( $p = 0.9280$ ) and dynActivation(SiLU) ( $p = 0.4485$ ) are statistically indistinguishable from the Mish variant, confirming that the dynActivation framework provides robust benefits regardless of the exact base function. Among external activations, Apa ( $p = 0.2598$ ), Trainable\_swish ( $p = 0.0581$ ), and Adaptive\_gelu ( $p = 0.0758$ ) perform competitively enough that their difference from the top rank is not strictly significant at the 0.05 threshold, though dynActivation(Mish) maintains a higher absolute mean accuracy in all cases.

Activation	<i>p</i> -Value	<i>t</i> -Statistic	Significant vs. Best
Apa [24]	0.2598	-1.2026	No
Trainable_swish [4]	0.0581	-2.1703	No
Pdelu [25]	0.1188	-1.7238	No
Melu [26]	0.0017	-4.4033	Yes
Mish [1]	0.0375	-2.4373	Yes
Prelu_scalar [6]	0.0208	-2.7976	Yes
Taaf [27]	0.0466	-2.3055	Yes
Adaptive_gelu [3]	0.0758	-2.0060	No
SiLU [35]	0.0649	-2.1020	No
Apl [28]	0.0474	-2.2952	Yes
GELU [3]	0.0535	-2.2207	No
Hardswish [37]	0.0406	-2.3893	Yes
ELU [39]	0.0019	-4.3338	Yes
CELU [33]	0.0019	-4.3345	Yes
Laaf_relu [29]	0.0386	-2.4202	Yes
ReLU [2]	0.0205	-2.8050	Yes
LeakyReLU [34]	0.0156	-2.9732	Yes
Srelu [30]	0.0002	-5.9098	Yes
SELU [8]	$4.20 \times 10^{-5}$	-7.3831	Yes
Softplus [36]	$5.70 \times 10^{-5}$	-7.0963	Yes
Saaf [31]	$1.10 \times 10^{-5}$	-8.7252	Yes
Tanh [38]	$0.00 \times 10^0$	-18.3604	Yes
Erfrelu [32]	0.0013	-4.6186	Yes
dynActivation(Mish)	-	-	No
dynActivation(GELU)	0.9280	-0.0929	No
dynActivation(SiLU)	0.4485	-0.7925	No
dynActivation(ReLU)	0.0140	-3.0425	Yes

Table 8: Statistical significance testing results against dynActivation(Mish), sorted ascending by p-value.

## 5.7 Local figure + local interpretation

Figure 4 plots each activation in accuracy-versus-loss space and connects each base activation to its dynamic counterpart. The plot reveals that dynamizing a base activation increases its final mean accuracy across the evaluated configurations. dynActivation(Mish) achieves the highest accuracy at 79.72%, displacing static Mish (78.91%) as the most accurate variant overall.

However, unlike the accuracy gains, the dynamic variants exhibit a slightly higher test loss compared to their static baselines (e.g., 0.6720 for dynActivation(Mish) versus 0.6348 for Mish). This indicates a trade-off where the dynamic variants achieve a higher absolute correct classification rate, but may produce slightly more confident incorrect predictions or slightly less confident correct predictions.

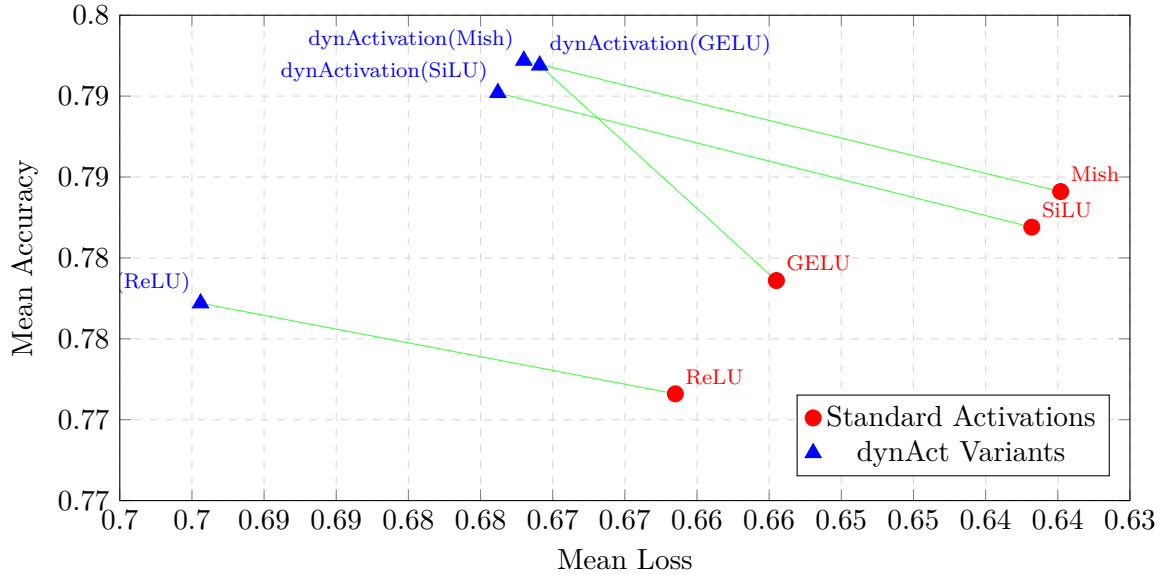


Figure 4: Accuracy-versus-Loss trade-off.

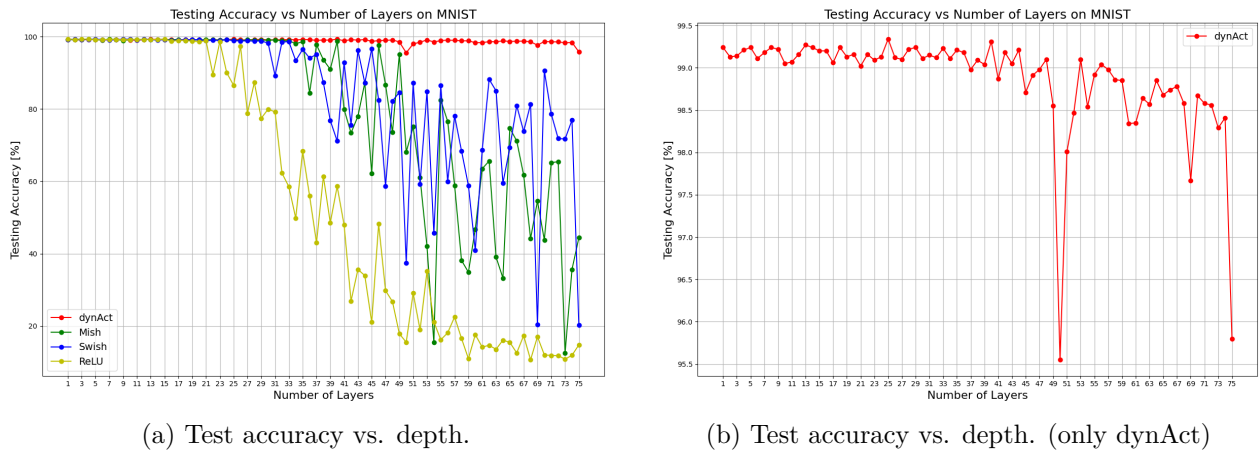
## 6 Overfitting Analysis on MNIST

### 6.1 Experimental setup for MNIST depth scaling

The MNIST analysis studies how model performance changes as network depth increases, using progressively deeper networks with two convolutional front-end layers and fully connected layers of fixed width. Batch normalization [11] and dropout [19] are included to reduce trivial training failures.

### 6.2 Depth scaling figure pair

Figure 5 (left) plots test accuracy from 1 to 75 layers for ReLU, Swish, Mish, and dynAct. dynAct (Mish base) is the only activation that never drops below 95% across the entire sweep, ranging between 95.3% and 99.3%. In contrast, ReLU collapses below 80% at approximately 25 layers and falls as low as 10–20% beyond 45 layers. Mish maintains near-99% accuracy up to about 15 layers before oscillating; it drops to approximately 60% at layers 40–50 and fluctuates between 40–80% at 50–75 layers. Swish begins degrading around 25–30 layers, oscillating between 40–80% and reaching approximately 40% by layer 75. The zoomed panel (right) sees some degradation of dynAct which seem negligible in comparison to the accuracy drop of the other activations.



(a) Test accuracy vs. depth.

(b) Test accuracy vs. depth. (only dynAct)

Figure 5: MNIST depth scaling figure pair.

### 6.3 Learned activation visualization

Figure 6 displays the learned per-layer activation shapes for the 50-layer MNIST network. Early convolutional layers adopt shapes close to the Mish base activation: `conv_1` converges to  $\alpha = 0.42$ ,  $\beta = -0.06$ ; `conv_2` to  $\alpha = 1.12$ ,  $\beta = -0.07$ . The early fully connected layers (layers 6–8) sustain strong nonlinearity with  $\alpha$  values of 1.05–1.39 and  $\beta$  near  $-0.06$  to  $-0.14$ . In the middle layers (14–30) a clear trend emerges:  $\alpha$  decreases to 0.41–0.60 while  $\beta$  increases to 0.51–0.57, pushing the activation toward near-linear behavior. Deep layers (30–45) consolidate at  $\alpha \approx 0.45$ –0.50,  $\beta \approx 0.51$ –0.55, retaining only a residual curvature from the Mish base. The final layers (46–49) display diverse specialized shapes with  $\alpha$  from 0.06 to 0.76 and  $\beta$  from  $-0.20$  to 0.39, suggesting task-specific fine-tuning near the output. This systematic transition from high- $\alpha$ /low- $\beta$  (Mish-like) in early layers to high- $\beta$ /low- $\alpha$  (near-linear) in deep layers is a quantitative expression of selective nonlinearity allocation. This way the network behaves more like a model of the size of 20 layers which in turn then seems reasonable why it performs so well, because all the activations perform favourably at this size.

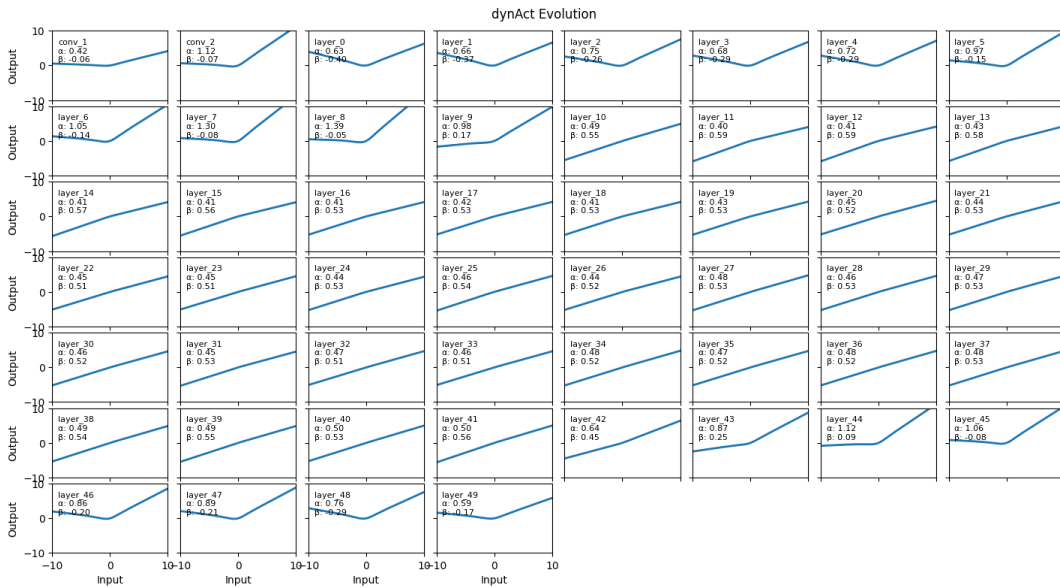


Figure 6: Learned layer-wise activation shapes for a 50-layer MNIST network.

### 6.4 Interpretation

The MNIST results provide direct evidence for the selective nonlinearity hypothesis. In the 50-layer network, the network transitions from Mish-like activations ( $\alpha \approx 1.1$ ,  $\beta \approx -0.07$ ) in early layers to near-linear behavior ( $\alpha \approx \beta \approx 0.5$ ) in middle and deep layers. Layers where  $\alpha \approx \beta$  satisfy  $f_i(x) \approx \beta_i x$ , which simplifies to a near-identity map for moderate input values, effectively creating learned skip connections within the activation. This mechanism reduces the effective curvature of deep layers without requiring explicit residual connections, which may explain the observed absence of depth-induced accuracy collapse. Notably, dynAct is the only activation maintaining  $> 95\%$  accuracy at 75 layers, consistent with its ability to adapt its depth-wise nonlinearity profile.

## 7 LLM Transfer Experiments

### 7.1 dynActGLU formulation

To test whether the dynActivation idea transfers beyond image models, this work adapts it to the feedforward block of a language model and proposes a new dynActGLU formulation following similar intuition as before. The static intermediate nonlinearity in the baseline GLU-type layer is replaced by a dynamic variant built on the same base function, preserving architectural comparability while isolating the effect of trainable activation behavior.

$$\text{FFN}_{\text{dynActGLU}}(x, W_1, V_\alpha, V_\beta, W_2) = ((\text{BaseAct}(xW_1) \odot (xV_\alpha - xV_\beta) + xW_1 \odot xV_\beta) \odot xW_1) W_2. \quad (10)$$

## 7.2 Short-run table

Table 9 reports validation loss and perplexity after 5,620 training steps.

Table 9: Short-run LLM results after 5620 training steps.

Activation	Loss	Perplexity
Baseline SwiGLU [13]	1.5072	4.5142
dynActGLU(Swish)	1.3979	4.0467

## 7.3 Long-run table

Table 10 reports validation loss and perplexity after 34,300 training steps.

Table 10: Long-run LLM results after 34300 training steps.

Activation	Loss	Perplexity
Baseline SwiGLU	1.3374	3.8091
dynActGLU(Swish)	1.3364	3.8056

# 8 Unified Evaluation

## 8.1 Stability tests

### 8.1.1 Initialization stability

The initialization-stability analysis tests different starting values for  $\alpha$  and  $\beta$  and reports both mean performance and instability.

Figure 7 confirms that the default initialization  $\alpha_{\text{init}} = 1$ ,  $\beta_{\text{init}} = 0$  achieves peak accuracy of 0.80. The same peak is reached at  $(\alpha = 2, \beta = 0)$ , and the majority of configurations yield accuracy in the range 0.78–0.80, demonstrating broad robustness to initialization. The only catastrophic failure occurs at  $(\alpha = 0, \beta = 0)$ , where accuracy collapses to 0.10—consistent with the activation degenerating to the zero function when both parameters vanish. Variance remains below 0.01 for most configurations, with a slightly elevated cluster near  $(\alpha = 0.5, \beta = -0.5)$ .

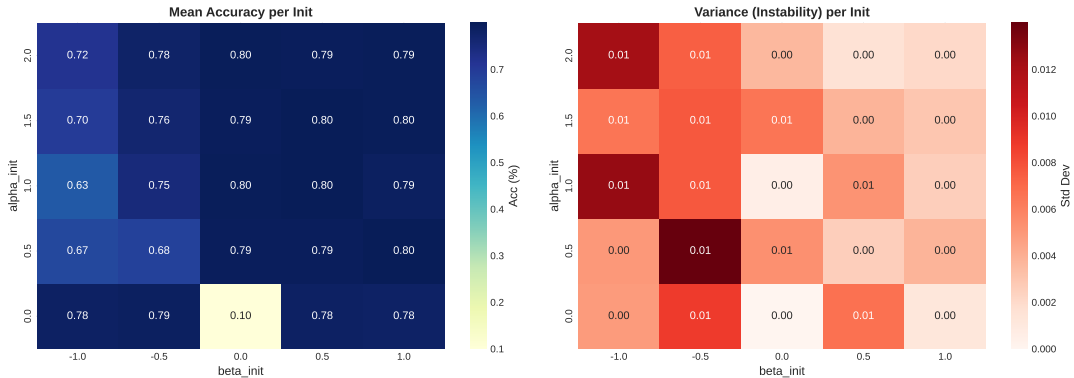


Figure 7: Initialization-ablation heatmap over  $\alpha_{\text{init}}$  and  $\beta_{\text{init}}$ .

### 8.1.2 Optimizer-/init-stability test

Across 27 configurations (3 initialization schemes  $\times$  3 optimizers  $\times$  3 learning rates) on CIFAR-10/ResNet18 [5], dynActivation(Mish) achieves the highest mean accuracy at 52.81% ( $\sigma = 25.18$ ), followed by Mish [1] at 49.47% (+3.34 pp advantage) and ReLU [2] at 42.25% (+10.56 pp advantage). The best single configuration for dynActivation(Mish) reaches 75.77% (kaiming\_normal initialization, RMSProp optimizer, lr = 0.001).

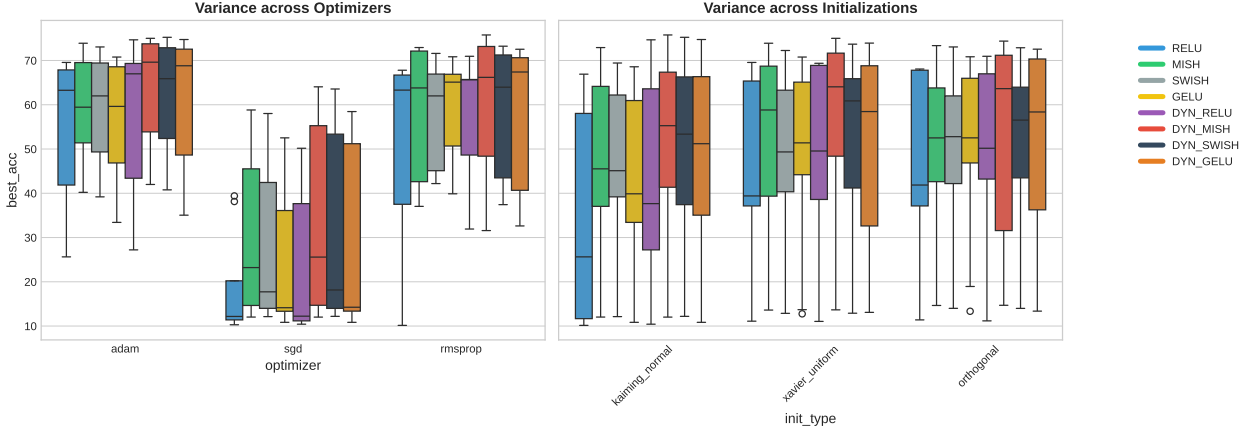


Figure 8: Variance across optimizers and initialization schemes.

### 8.1.3 Hyperparameter-stability test

dynActivation is tested on multiple learning rates, batch sizes and weight decay levels to test for hyperparameter robustness so that the a good run is not just a lucky run.

It can be shown that the dynActivation-family can maintain its performance advantage despite different hyperparameters suggesting a good robustness against variations in them.

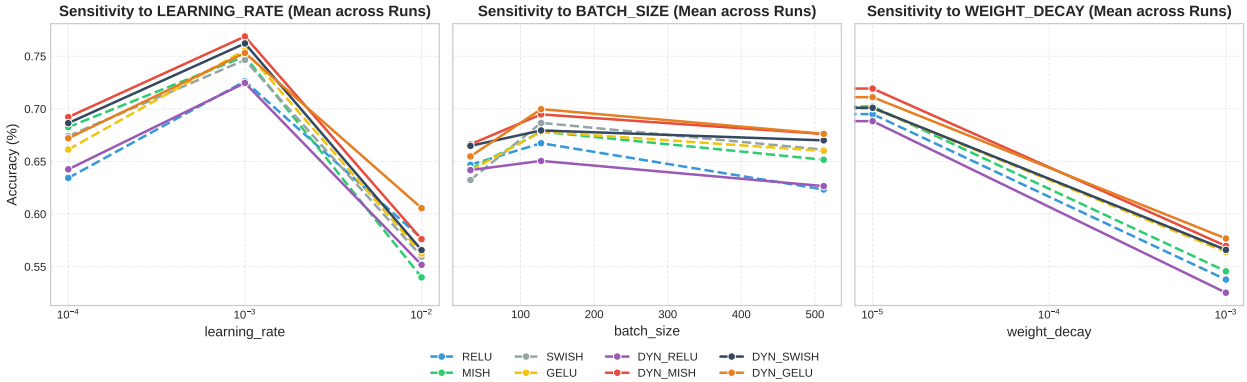


Figure 9: Robustness across hyperparameters.

### 8.1.4 Monotonicity / curvature test

Figure 10 shows the trajectories of mean and variance of  $\alpha$  and  $\beta$  over 30 training epochs.  $\bar{\alpha}$  starts near 0.90 at epoch 1, drops sharply to  $\approx 0.80$  by epoch 5, and converges to  $\approx 0.75$  by epoch 10–15, where it remains stable. The variance band for  $\alpha$  is initially narrow, widens to a range of approximately 0.65–0.87 during epochs 5–10, then stabilizes at  $\pm 0.10$  around the mean.  $\bar{\beta}$  starts near  $-0.05$  at epoch 1, shifts to  $\approx -0.08$  by epoch 5, and stabilizes there through epoch 30. The variance band for  $\beta$  is substantially larger ( $\pm 0.2$  around the mean throughout training), indicating that different layers specialize their linear-path parameter to a much greater degree than

the nonlinearity-scaling parameter. Both parameters reach their converged regime by approximately epoch 10–15, demonstrating rapid and stable adaptation with no ongoing drift.

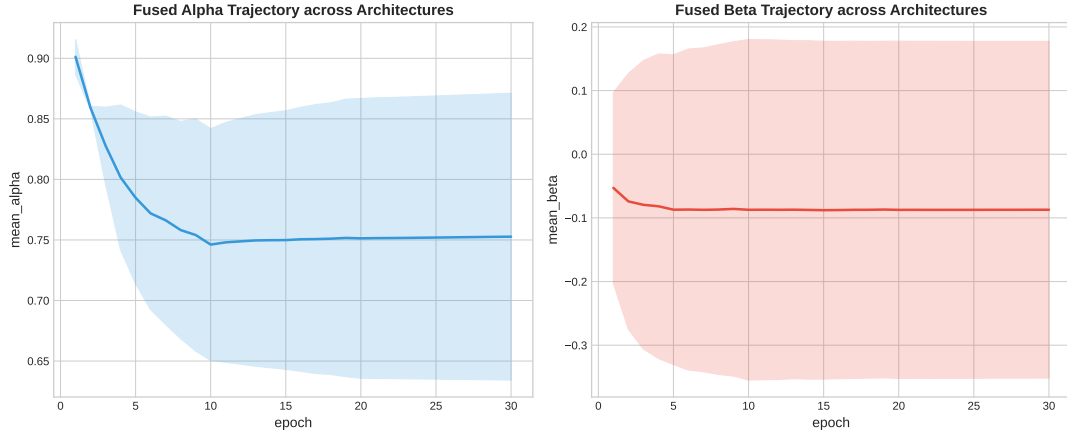


Figure 10: Trajectories of mean and variance of activation parameters across epochs.

## 8.2 Robustness tests

### 8.2.1 Distribution-shift test

Figure 11 plots accuracy across four corruption types [18] (Gaussian noise, Gaussian blur, brightness, contrast) at five severity levels. Under Gaussian noise at severity 1, dynActivation(Mish) leads with 52.14%, outperforming ReLU (49.72%) by +2.42 pp and Mish (50.26%) by +1.88 pp. Under brightness perturbation at severity 5, dynActivation(Mish) achieves 51.84%, the highest among all activations, exceeding ReLU by +4.02 pp (47.82%). However, under contrast corruption, dynActivation(Mish) falls behind: at severity 1, Swish leads at 45.38% while dynActivation(Mish) reaches only 41.00% (−4.38 pp); at severity 5, Mish achieves 18.14% versus 16.58% for dynActivation(Mish). The overall pattern is mixed: dynActivation(Mish) shows clear advantages under noise and brightness corruptions, while exhibiting a moderate disadvantage under contrast perturbations. The additional trainable parameters do not introduce a uniform vulnerability but shift the degradation profile in a corruption-type-dependent manner.

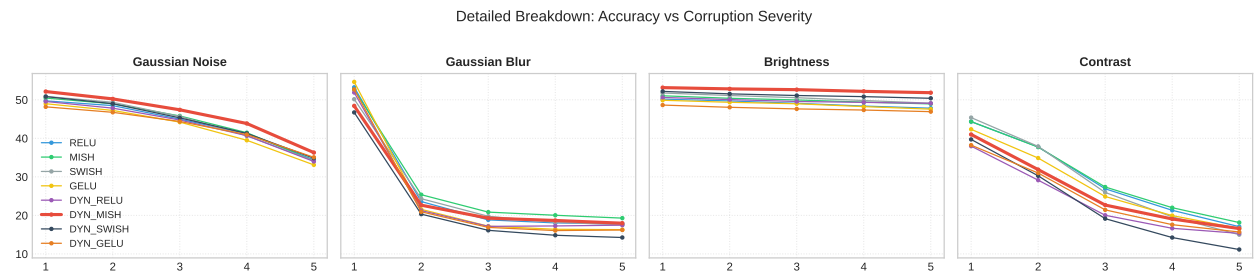


Figure 11: Distribution-shift robustness across corruption types and severities.

### 8.2.2 Adversarial-robustness test

Figure 12 reports accuracy drop under FGSM [9] and PGD [10] attacks at multiple perturbation budgets on CIFAR-10/ResNet18. Under FGSM at  $\epsilon = 0.01$ , dynActivation(Mish) achieves the lowest accuracy drop at 40.56%, compared to 45.29% for GELU [3], a 4.73 pp advantage. At  $\epsilon = 0.08$ , dynActivation(Mish) sustains a 55.39% drop versus 62.79% for ReLU (7.40 pp advantage), 63.67% for Mish (8.28 pp), and 63.95% for Swish (8.56 pp). Under PGD at  $\epsilon = 0.02$ , dynActivation(Mish) drops 64.76% versus 69.34% for ReLU, a 4.58 pp margin. At PGD  $\epsilon = 0.04$ , dynActivation(Mish) achieves 80.39% drop versus 82.11% for ReLU (1.72 pp) and 82.36% for Mish (1.97 pp). These

results indicate that dynActivation(Mish) is the most adversarially robust variant, with the largest margins under high-budget FGSM attacks and consistent but smaller improvements under PGD.

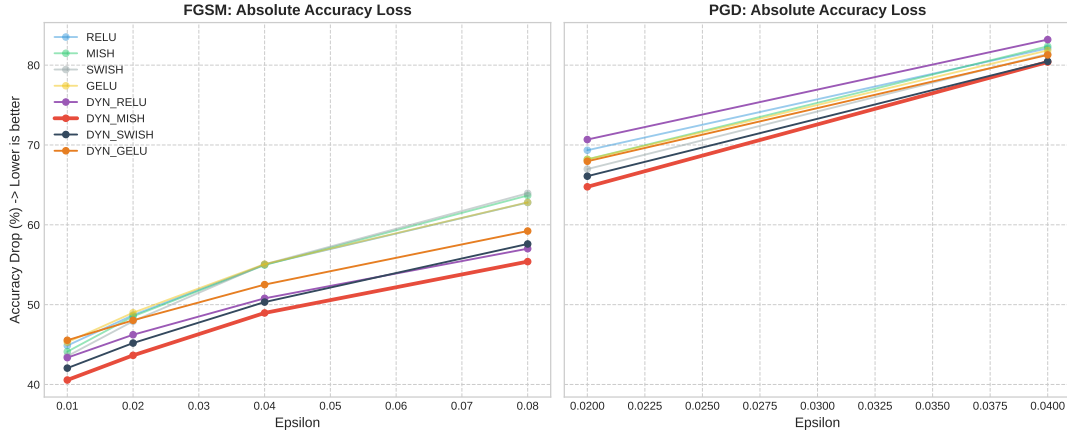


Figure 12: Adversarial robustness under FGSM and PGD.

### 8.2.3 Regularization ablation

The no-penalty baseline achieves 79.82% accuracy. L1 regularization at  $\lambda = 10^{-5}$  yields 78.91%, improving to 79.11% at  $\lambda = 10^{-4}$  and peaking at 80.02% at  $\lambda = 10^{-3}$ . L2 follows a flatter trajectory: 79.80% at  $\lambda = 10^{-5}$ , 79.34% at  $\lambda = 10^{-4}$ , and 79.92% at  $\lambda = 10^{-3}$ . The best configuration (L1,  $\lambda = 10^{-3}$ ) achieves +0.20 pp over the baseline, with learned parameters  $\bar{\alpha} = 0.1319$  and  $\bar{\beta} = 0.0124$ , indicating substantial parameter shrinkage toward near-linear behavior. The accuracy optimum at moderate regularization preserves parameter diversity while providing a small but consistent accuracy improvement, suggesting that sparse regularization toward near-linear shapes is beneficial but that collapsing the parameters fully overshoots the optimum.

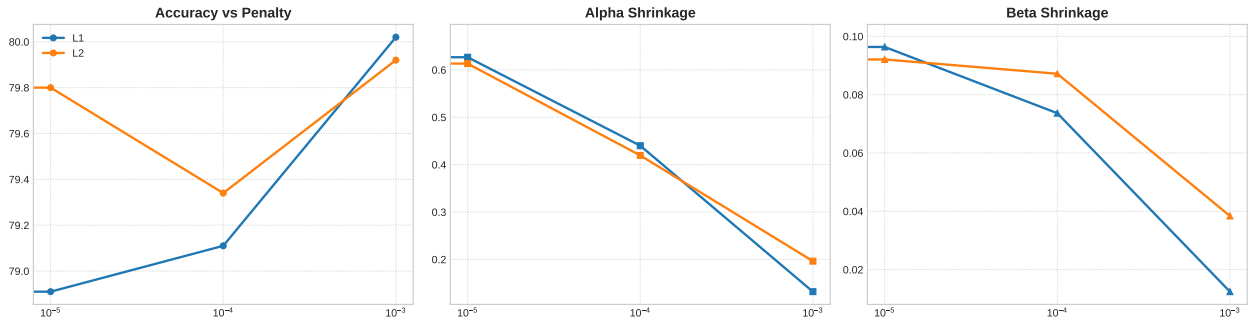


Figure 13: L1 and L2 Regularization on dynActivation Parameters.

### 8.3 Efficiency tests

#### 8.3.1 Convergence test



Figure 14: AUC-based convergence comparison.

Table 11 summarizes the quantitative convergence comparison. `dynActivation(Mish)` achieves the lowest AUC at 2120, a 24% reduction relative to static Mish (2785) and a 26% reduction relative to static ReLU (2864). `dynActivation(GELU)` (AUC 2138) and `dynActivation(SiLU)` (AUC 2170) also substantially outperform all static baselines. On threshold-based metrics, `dynActivation(GELU)` reaches training loss 0.5 fastest, requiring only 711 steps versus 781 for static GELU and ReLU. These results confirm that dynamization consistently accelerates loss reduction, with the ordering `dynActivation(Mish)` < `dynActivation(GELU)` < `dynActivation(SiLU)` < `dynActivation(ReLU)` < `GELU` < `Mish` < `ReLU` for the AUC metric.

Table 11: Theory-convergence statistics across activations.

Activation	AUC Loss	Steps to 1.0	Steps to 0.5	Conv. rate
relu	2864.364252	277	781	0.000206
mish	2784.969175	204	835	0.000203
swish	2830.302696	293	835	0.000211
gelu	2605.357465	204	781	0.000209
<code>dynActivation(ReLU)</code>	2350.585219	257	781	0.000213
<code>dynActivation(Mish)</code>	2119.673199	226	781	0.000213
<code>dynActivation(SiLU)</code>	2170.423420	245	835	0.000221
<code>dynActivation(GELU)</code>	2137.512088	204	711	0.000215

#### 8.3.2 Runtime benchmark

Eventhough `dynActivation`-variants seem to provide some performance improvements, they also introduce computational overhead because of the additional parameters and gradient pathways.

Figure 15 measures forward and backward times across device types, numeric precision, batch size, and input dimension.

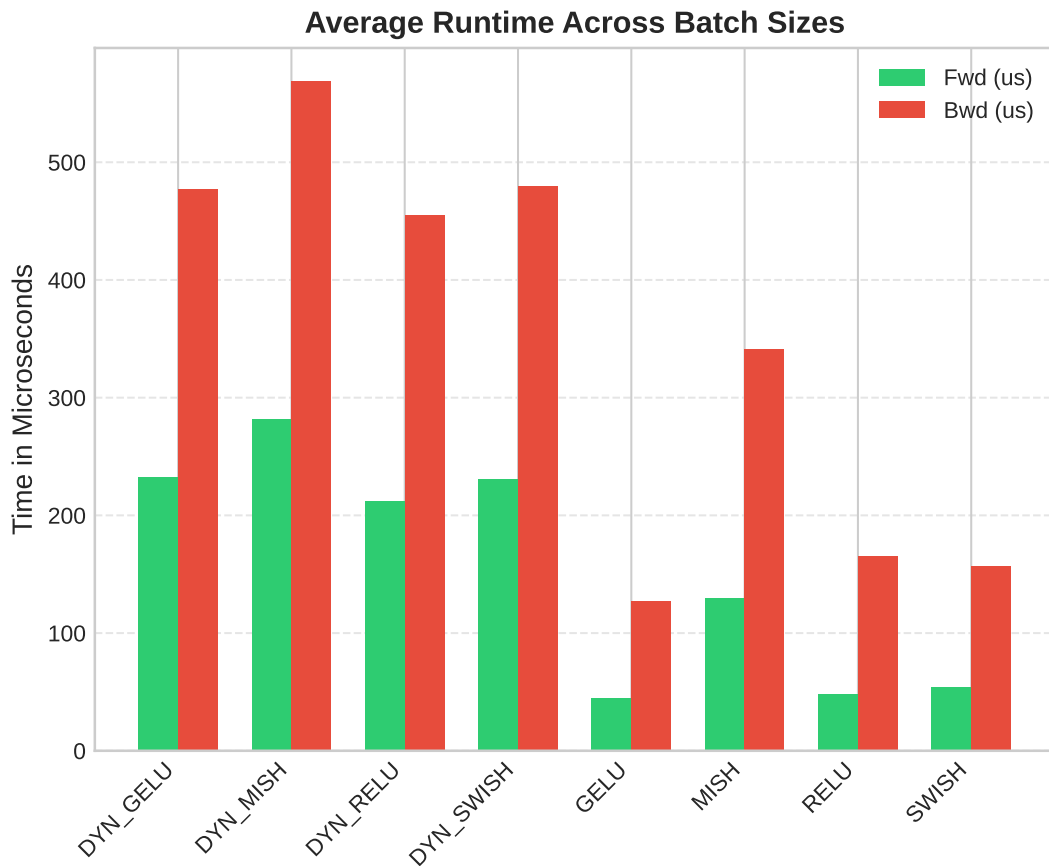


Figure 15: Operator-level runtime benchmark.

### 8.3.3 Training-efficiency test

But the runtime has to be seen in relation with the convergence rate of the model to allow a conclusion if the computational overhead is worth it. Figure 16 combines convergence behavior with hardware-level throughput. This graphic shows that the increased convergence speed seems to outweigh the computational overhead and suggests that the dynActivation variants are up to 54% more efficient to train than normal ReLU.

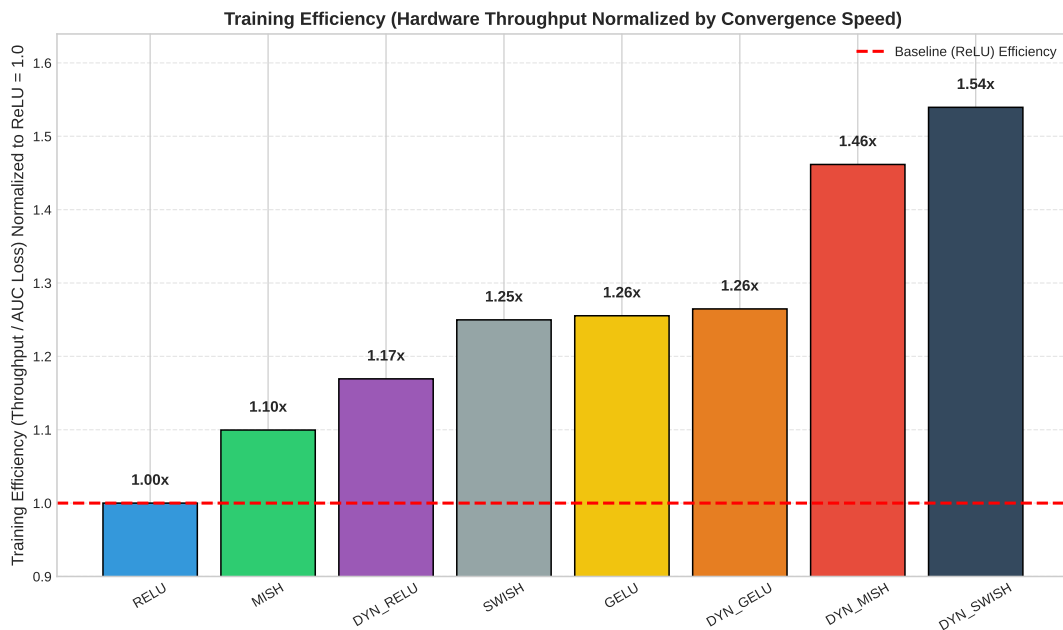


Figure 16: Training efficiency combining convergence and compute cost.

## 9 Discussion

**CIFAR classification.** The +14.02 pp improvement on CIFAR-10/AttentionCNN (from 64.25% Mish to 78.27% dynActivation(Mish)) and the +12.39 pp gain on CIFAR-100/AttentionCNN (from 33.31% ReLU to 45.70% dynActivation(GELU)) are the largest individual gains observed. These margins suggest that some architectures are particularly constrained by a fixed activation; adding two learnable parameters per layer is sufficient to substantially improve performance. Across the broader 27-activation sweep, dynActivation(Mish) places first at 79.72%. The unified paired testing shows that this advantage is statistically significant over its static counterpart Mish ( $p = 0.0375$ ), as well as over established standards like ReLU ( $p = 0.0205$ ) and SELU ( $p = 4.20 \times 10^{-5}$ ). The only activations performing statistically on par with the leading variant are other members of the dynActivation family (GELU, SiLU).

**Depth scaling.** The fact that dynAct is the only activation maintaining  $> 95\%$  accuracy from 1 to 75 layers—while all static baselines collapse below 60% before layer 50—cannot be attributed to a simple accuracy offset. The layer-wise shape analysis explains the mechanism: the network learns to reduce  $\alpha$  and increase  $\beta$  in deep layers, producing near-identity activations ( $\alpha \approx \beta \approx 0.5$ ) that act as effective skip connections without architectural modification. This transition from  $\alpha \approx 1.12$  in early layers to  $\alpha \approx 0.45\text{--}0.50$  in layers 30–45 is a continuous, task-driven interpolation between nonlinear and linear behavior.

**Learned parameter trajectories and selective nonlinearity.** The parameter trajectory (Figure 10) confirms that  $\bar{\alpha}$  converges from 0.90 to 0.75 by epoch 10, while  $\bar{\beta}$  stabilizes at  $-0.08$  by epoch 5. The converged values correspond to a slightly attenuated Mish nonlinearity with a small negative linear correction, a regime that the network consistently selects across architectures. The large inter-layer variance in  $\beta$  ( $\pm 0.2$ ) versus the smaller variance in  $\alpha$  ( $\pm 0.10$ ) indicates that the linear-path parameter is the primary instrument of layer-wise specialization, while the nonlinearity-scaling parameter converges to a more uniform global value.

**Adversarial robustness and convergence.** The adversarial advantage under FGSM [9] at  $\varepsilon = 0.08$ —where dynActivation(Mish) reduces accuracy drop by 7.40 pp relative to ReLU [2] (55.39% vs. 62.79%), 8.28 pp relative to Mish, and 8.56 pp relative to Swish—is consistent with the hypothesis that a smoother, partially linearized activation reduces the network’s local sensitivity to input perturbations. The 24% convergence-AUC reduction (2120 vs. 2785 for Mish) indicates that the gradient advantage observed in 50-layer networks translates into a practical training-time benefit under standard experimental protocols.

**LLM transfer.** The 10.3% relative perplexity reduction after 5,620 steps provides evidence that the dynActivation idea is not image-specific. The near-zero residual gap at 34,300 steps (3.806 vs. 3.809) is consistent with asymptotic equivalence rather than a long-run regression, and the short-run advantage may be practically important in low-compute training regimes.

**Optimizer and initialization stability.** Across 27 optimizer–init–learning-rate configurations, dynActivation(Mish) achieves the highest mean accuracy (52.81%), leading Mish by +3.34 pp and ReLU by +10.56 pp. The best single configuration (kaiming\_normal, RMSProp, lr = 0.001) reaches 75.77%. This consistent advantage suggests that dynActivation is a robust drop-in replacement rather than a method requiring careful co-optimization of the training protocol.

**Distribution-shift robustness.** The distribution-shift evaluation [18] reveals a mixed rather than neutral picture: dynActivation(Mish) leads under Gaussian noise (+2.42 pp over ReLU at severity 1) and brightness corruptions (+4.02 pp over ReLU at severity 5), but falls behind under contrast perturbations ( $-4.38$  pp vs. Swish at severity 1). This corruption-type-dependent profile warrants further investigation into whether the learned parameter regime can be regularized toward more uniform robustness.

## 10 Limitations

Several limitations qualify the claims made in this paper. First, while dynActivation(Mish) achieves the highest mean accuracy overall, its advantage over Apa is not yet statistically significant in the

aggregated paired setting. Further testing is needed to proof the statistical significance of the empirical results.

Second, the LLM perplexity advantage of 10.3% after 5,620 steps collapses to 0.09% at 34,300 steps, making the long-run benefit effectively zero; dynActivation in language models should therefore be framed as a convergence accelerator rather than an asymptotic improvement.

Third, while the two additional parameters per layer are lightweight, the computational overhead relative to static activations has not been eliminated; the runtime benchmark quantifies this cost and it must be weighed against the accuracy gains in latency-sensitive applications.

Fourth, the current understanding of why  $\bar{\alpha}$  and  $\bar{\beta}$  converge to these specific values rests on an empirical observation rather than a theoretical guarantee; a principled analysis of the optimization landscape that explains these attractors is left for future work.

## References

- [1] D. Misra. Mish: A self regularized non-monotonic activation function. In *Proceedings of the British Machine Vision Conference (BMVC)*, 2020. <https://arxiv.org/abs/1908.08681>
- [2] V. Nair and G. E. Hinton. Rectified linear units improve restricted Boltzmann machines. In *Proceedings of the 27th International Conference on Machine Learning (ICML)*, pp. 807–814, 2010.
- [3] D. Hendrycks and K. Gimpel. Gaussian error linear units (GELUs). *arXiv preprint arXiv:1606.08415*, 2016. <https://arxiv.org/abs/1606.08415>
- [4] P. Ramachandran, B. Zoph, and Q. V. Le. Searching for activation functions. *arXiv preprint arXiv:1710.05941*, 2017. <https://arxiv.org/abs/1710.05941>
- [5] K. He, X. Zhang, S. Ren, and J. Sun. Deep residual learning for image recognition. In *Proceedings of the IEEE Conference on Computer Vision and Pattern Recognition (CVPR)*, pp. 770–778, 2016. <https://arxiv.org/abs/1512.03385>
- [6] K. He, X. Zhang, S. Ren, and J. Sun. Delving deep into rectifiers: Surpassing human-level performance on ImageNet classification. In *Proceedings of the IEEE International Conference on Computer Vision (ICCV)*, pp. 1026–1034, 2015.
- [7] D.-A. Clevert, T. Unterthiner, and S. Hochreiter. Fast and accurate deep network learning by exponential linear units (ELUs). In *Proceedings of the 4th International Conference on Learning Representations (ICLR)*, 2016. <https://arxiv.org/abs/1511.07289>
- [8] G. Klambauer, T. Unterthiner, A. Mayr, and S. Hochreiter. Self-normalizing neural networks. In *Advances in Neural Information Processing Systems (NeurIPS)*, pp. 971–980, 2017. <https://arxiv.org/abs/1706.02515>
- [9] I. J. Goodfellow, J. Shlens, and C. Szegedy. Explaining and harnessing adversarial examples. In *Proceedings of the 3rd International Conference on Learning Representations (ICLR)*, 2015. <https://arxiv.org/abs/1412.6572>
- [10] A. Madry, A. Makelov, L. Schmidt, D. Tsipras, and A. Vladu. Towards deep learning models resistant to adversarial attacks. In *Proceedings of the 6th International Conference on Learning Representations (ICLR)*, 2018. <https://arxiv.org/abs/1706.06083>
- [11] S. Ioffe and C. Szegedy. Batch normalization: Accelerating deep network training by reducing internal covariate shift. In *Proceedings of the 32nd International Conference on Machine Learning (ICML)*, pp. 448–456, 2015. <https://arxiv.org/abs/1502.03167>
- [12] D. P. Kingma and J. Ba. Adam: A method for stochastic optimization. In *Proceedings of the 3rd International Conference on Learning Representations (ICLR)*, 2015. <https://arxiv.org/abs/1412.6980>
- [13] N. Shazeer. GLU variants improve transformer. *arXiv preprint arXiv:2002.05202*, 2020. <https://arxiv.org/abs/2002.05202>
- [14] A. Krizhevsky. Learning multiple layers of features from tiny images. Technical report, University of Toronto, 2009. <https://www.cs.toronto.edu/~kriz/cifar.html>
- [15] L. Deng. The MNIST database of handwritten digit images for machine learning research. *IEEE Signal Processing Magazine*, 29(6):141–142, 2012. <https://ieeexplore.ieee.org/document/6296535>

- [16] A. G. Howard, M. Zhu, B. Chen, D. Kalenichenko, W. Wang, T. Weyand, M. Andreetto, and H. Adam. MobileNets: Efficient convolutional neural networks for mobile vision applications. *arXiv preprint arXiv:1704.04861*, 2017. <https://arxiv.org/abs/1704.04861>
- [17] G. Huang, Z. Liu, L. van der Maaten, and K. Q. Weinberger. Densely connected convolutional networks. In *Proceedings of the IEEE Conference on Computer Vision and Pattern Recognition (CVPR)*, pp. 4700–4708, 2017. <https://arxiv.org/abs/1608.06993>
- [18] D. Hendrycks and T. Dietterich. Benchmarking neural network robustness to common corruptions and perturbations. In *Proceedings of the 7th International Conference on Learning Representations (ICLR)*, 2019. <https://arxiv.org/abs/1903.12261>
- [19] N. Srivastava, G. Hinton, A. Krizhevsky, I. Sutskever, and R. Salakhutdinov. Dropout: A simple way to prevent neural networks from overfitting. *Journal of Machine Learning Research*, 15(56):1929–1958, 2014. <https://jmlr.org/papers/v15/srivastava14a.html>
- [20] PleIAs. Monad: A 56M-parameter generalist small reasoning model. Model card, Hugging Face, 2025. <https://huggingface.co/PleIAs/Monad>
- [21] K. Biswas, A. Reza, M. Karri, D. Jha, H. Pan, and U. Bagci. Optimizing neural network effectiveness via non-monotonicity refinement. In *Proceedings of the IEEE/CVF Winter Conference on Applications of Computer Vision (WACV)*, 2025. [https://openaccess.thecvf.com/content/WACV2025/papers/Biswas\\_Optimizing\\_Neural\\_Network\\_WACV\\_2025\\_paper.pdf](https://openaccess.thecvf.com/content/WACV2025/papers/Biswas_Optimizing_Neural_Network_WACV_2025_paper.pdf)
- [22] Anonymous. Smooth activations and reproducibility in deep networks. *Under review at ICLR 2021*, 2021. <https://openreview.net/pdf/91eaf16733eb3caa4805b03b1eccc819954eafc3.pdf>
- [23] *A study of convolutional neural networks with attention. Procedia Computer Science*, 2021. <https://www.sciencedirect.com/science/article/pii/S1877050921011340>
- [24] K. Pikoulis et al., “Adaptive parametric activation,” *arXiv preprint arXiv:2407.08567*, 2024.
- [25] Q. Cheng, H. Li, Q. Wu, L. Ma, and K. N. Ngan, “Parametric deformable exponential linear units for deep neural networks,” *Neural Networks*, vol. 125, pp. 281–289, 2020.
- [26] L. Nanni et al., “Comparison of different convolutional neural network activation functions and methods for building ensembles,” *SN Computer Science*, 2022.
- [27] M. A. A. S. Al-Shami, “The analog activation function (TAAF) of emergent linear systems,” *Preprints*, 2024.
- [28] F. Agostinelli, M. Hoffman, P. Sadowski, and P. Baldi, “Learning activation functions to improve deep neural networks,” *arXiv preprint arXiv:1412.6830*, 2014.
- [29] A. D. Jagtap, K. Kawaguchi, and G. E. Karniadakis, “Locally adaptive activation functions with slope recovery for deep and physics-informed neural networks,” *Proceedings of the Royal Society A*, vol. 476, no. 2239, p. 20200334, 2020.
- [30] X. Jin, C. Xu, J. Feng, Y. Wei, J. Xiong, and S. Yan, “Deep learning with s-shaped rectified linear activation units,” *arXiv preprint arXiv:1512.07030*, 2015.
- [31] Y. Yang et al., “Shape autotuning activation function,” *Expert Systems with Applications*, vol. 168, 2021.
- [32] A. Rajanand et al., “ErfReLU: Adaptive activation function for deep neural network,” *arXiv preprint arXiv:2306.01822*, 2023.

- [33] J. T. Barron, “Continuously differentiable exponential linear units,” *arXiv preprint arXiv:1704.07483*, 2017.
- [34] A. L. Maas, A. Y. Hannun, and A. Y. Ng, “Rectifier nonlinearities improve neural network acoustic models,” in *Proc. ICML*, vol. 30, no. 1, 2013, p. 3.
- [35] S. Elfving, E. Uchibe, and K. Doya, “Sigmoid-weighted linear units for neural network function approximation in reinforcement learning,” *Neural Networks*, vol. 107, pp. 3–11, 2018.
- [36] C. Dugas, Y. Bengio, F. Bélisle, C. Nadeau, and R. Garcia, “Incorporating second-order functional knowledge for better option pricing,” in *Advances in Neural Information Processing Systems*, vol. 13, 2001.
- [37] A. Howard et al., “Searching for mobilenetv3,” in *Proceedings of the IEEE/CVF International Conference on Computer Vision*, 2019.
- [38] Y. LeCun, L. Bottou, G. B. Orr, and K.-R. Müller, “Efficient backprop,” *Neural networks: Tricks of the trade*, pp. 9–50, 1998.
- [39] D.-A. Clevert, T. Unterthiner, and S. Hochreiter, “Fast and accurate deep network learning by exponential linear units (elus),” *arXiv preprint arXiv:1511.07289*, 2015.

## Use of generative AI

Generative AI tools, primarily Perplexity (GPT-5.4 and Gemini 3.1 Pro), were used as support tools for language refinement, drafting assistance, preparation of selected figures and tests. Any AI-generated suggestions or draft materials were critically reviewed, revised, and verified by the author. All scientific reasoning, experimental design, analysis, and final interpretation were conducted and verified by the author. The author takes full responsibility for the content of this manuscript.